OPEN ACCESS
JOURNAL OF ADVANCED DIELECTRICS
Vol. 12, No. 6 (2022) 2250017 (8 pages)

DOI: 10.1142/S2010135X22500175

Achieving both large piezoelectric constant and low dielectric loss in $BiScO_3$–$PbTiO_3$–$Bi(Mn_{2/3}Sb_{1/3})O_3$ high-temperature piezoelectric ceramics

Yunyun Feng, Changhong Yang*, Xiaoying Guo, Wei Sun, Wenxuan Wang, Xiujuan Lin and Shifeng Huang†

Shandong Provincial Key Laboratory of Preparation and Measurement of Building Materials University of Jinan, Jinan 250022, P. R. China

*mse_yangch@ujn.edu.cn
†mse_huangf@ujn.edu.cn

Received 13 July 2022; Revised 30 August 2022; Accepted 8 September 2022; Published 26 October 2022

$BiScO_3$–$PbTiO_3$ binary ceramics own both high Curie temperature and prominent piezoelectric properties, while the high dielectric loss needs to be reduced substantially for practical application especially at high temperatures. In this work, a ternary perovskite system of $(1–x–y)BiScO_3$–$yPbTiO_3$–$xBi(Mn_{2/3}Sb_{1/3})O_3$ (BS–*y*PT–*x*BMS) with $x = 0.005$, $y = 0.630$–0.645 and $x = 0.015$, $y = 0.625$–0.640 was prepared by the traditional solid-state reaction method. The phase structure, microstructure, dielectric/piezoelectric/ferroelectric properties were studied. Among BS–*y*PT–*x*BMS ceramic series, the BS–0.630PT–0.015BMS at morphotropic phase boundary possesses the reduced dielectric loss factor ($\tan\delta = 1.20\%$) and increased mechanical quality factor ($Q_m = 84$), and maintains a high Curie temperature ($T_C = 410$°C) and excellent piezoelectric properties ($d_{33} = 330$ pC/N) simultaneously. Of particular importance, at elevated temperature of 200°C, the value of $\tan\delta$ is only increased to 1.59%. All these properties indicate that the BS–0.630PT–0.015BMS ceramic has great potential for application in high-temperature piezoelectric devices.

Keywords: High-temperature piezoelectric ceramics; $BiScO_3$–$PbTiO_3$; morphotropic phase boundary; $Bi(Mn_{2/3}Sb_{1/3})O_3$.

1. Introduction

Piezoelectric functional materials have broad applications in various industrial devices, such as piezoelectric sensors, actuators, and transducers. However, with the rapid development of automotive manufacturing, energy exploration, aerospace, and other fields, there is an urgent demand for high-temperature piezoelectric materials ($T \geq 200$°C).[1–6] Lead zirconate titanate $Pb(Zr,Ti)O_3$ (PZT) piezoelectric ceramics have been occupying the market of commercial piezoelectric devices due to their competitive comprehensive properties, rich component adjustability, and simple preparation process. However, the low Curie temperatures T_C ($T_C \leq 370$°C) of PZT systems restrict their applications at only below 170°C.[7–11] Therefore, the traditional PZT ceramics cannot meet the use requirements for high temperatures.

Aiming at the high-temperature application field, the explorations of various piezoelectric ceramic systems have been carried out, such as Bi_3TiNbO_9 ($T_C = 907$°C, $d_{33} = 3$ pC/N),[12] $Na_{0.5}Bi_{4.5}Ti_4O_{15}$ ($T_C = 657$°C, $d_{33} = 16$ pC/N),[13] and $Bi(Me)O_3$–$PbTiO_3$ (Me = Sc, In, Yb, Mg/Ti, Fe and Ga).[14] Among them, the $BiScO_3$–$PbTiO_3$ ceramic systems have attracted increasing research interest. Especially, a large piezoelectric coefficient ($d_{33} = 460$ pC/N) and a high Curie temperature ($T_C = 450$°C) have been obtained simultaneously in $0.36BiScO_3$–$0.64PbTiO_3$ (0.36BS–0.64PT) with morphotropic phase boundary (MPB) composition,[15] indicating the great potential for high-temperature applications. However, the high dielectric loss factor ($\tan\delta > 3\%$) and low mechanical quality factor ($Q_m < 30$) are obtained for 0.36BS–0.64PT ceramic and other BS–PT compositions,[16] severely limiting their applications as electronic devices at high temperatures due to the high energy consumption and high heat dissipation. To improve the overall performances, great efforts have been made by composition regulation, such as doping with La, Zr, Mn, and other single elements,[17–20] or introducing a third component such as $Pb(Mn_{1/3}Sb_{2/3})O_3$, $Pb(Zn_{1/3}Nb_{2/3})O_3$, and $Pb(Mg_{1/3}Nb_{2/3})O_3$.[21–23] Unfortunately, the modification is often accompanied by a serious decrease in Curie temperature or piezoelectric constant. For example, the reported $0.34BS–0.65PT–0.01Pb(Mn_{1/3}Sb_{2/3})O_3$ has a reduced $\tan\delta$ of 1.13%@50°C and slightly decreased T_C of 422°C, while the d_{33} is only 200 pC/N at room temperature and the $\tan\delta$ is over 10% at 200°C.[21] Another composition of $0.33BS–0.60PT–0.07Pb(Mn_{1/3}Sb_{2/3})O_3$ exhibits a low $\tan\delta$ of 1.4% at room temperature, while both d_{33} of 225 pC/N and T_C of 330°C are seriously attenuated.[24] Therefore, how to make a good balance among piezoelectric constant, Curie temperature and $\tan\delta$ for BS–PT ceramics remains a big challenge.

In this work, a novel ternary $(1–x–y)BiScO_3$–$yPbTiO_3$–$xBi(Mn_{2/3}Sb_{1/3})O_3$ (abbreviated as BS–*y*PT–*x*BMS) ceramic system with $x = 0.005$, $y = 0.630$–0.645 and $x = 0.015$, $y = 0.625$–0.640 was designed. The selection of Bi-based end

*Corresponding author.

member $Bi(Mn_{2/3}Sb_{1/3})O_3$ as a third component is mainly based on the following factors: (i) The Mn and Sb elements can realize the effects of soft and hard co-doping. (ii) Bi substitution for Pb plays a crucial role in enhancing tetragonality and polarizability at the MPB.[25] (ii) The volatilization of Bi at high-temperature sintering process is only one-tenth of Pb in $BiScO_3$–$PbTiO_3$ ceramics.[26] Via the component design approach, the dielectric loss decreases dramatically, and Curie temperature and piezoelectric performance maintain well simultaneously. Particularly, the BS–0.630PT–0.015BMS with MPB composition displays excellent overall properties with an ultralow tanδ (1.20%@25°C, 1.59%@200°C), large value of piezoelectric coefficient (d_{33} = 330 pC/N), and high Curie temperature (T_C = 410°C). All these characteristics make BS–0.630PT–0.015BMS more appropriate for high-temperature usage.

2. Experimental Procedure

Series of BS–*y*PT–*x*BMS ceramics were prepared by conventional solid-state reaction methods. The raw materials, Sb_2O_3 (99.5%), Bi_2O_3 (99.9%), $MnCO_3$ (99.9%), Sc_2O_3 (99.9%), PbO (99.9%), TiO_2 (99.0%), were weighed according to the stoichiometric ratio with 1% Bi_2O_3 and 2% PbO excess to coordinate the evaporation of bismuth (Bi) and lead (Pb) in the sintering process. The above mixtures were wetly milled together with zirconia balls for 24 h in an ethanol media. The milled powder was dried at 70°C for 5 h and calcined in an alumina crucible at 800°C for 2 h. After sieving through 60 mesh (Φ = 250 μm), the powder added with a binder of polyvinyl alcohol (PVA) was pressed into pellets ($\Phi 10 \times 1$ mm^3) at a pressure of 6 MPa for 1 min. PVA was burned off at 600°C for 2 h at a heating rate of 3°C/min. Then, the green disks embedded in alumina powder were sintered at 1040°C for 2 h at a heating rate of 4°C/min and cooled at a rate of 5°C/min. The samples were polished, cleaned, coated with silver, and sintered at 560°C for 30 min successively. Finally, the pellets were poled at 140°C under an electric field of 40 kV/cm for 20 min in silicone oil for electrical measurements.

The phase structure of sintered ceramic sample was characterized by X-ray diffraction in the range of 2θ from 20° to 60° (XRD, D8 ADVANCE, Bruker, Germany). The fracture surface microstructure was characterized by scanning electron microscope (SEM, EVOLS15, Zeiss, Germany). Measurement of density was carried by Archimedes drainage method using electron densitometer (DK-300A). The piezoelectric constant d_{33} was obtained by the quasi-static meter (ZJ-6A, Institute of Acoustics, Chinese Academy of Sciences, Beijing, China). Both dielectric constant and tanδ were measured at a frequency of 1 kHz in a temperature range from room temperature to 500°C by using an impedance analyzer (Agilent 4294A, Agilent, Santa Clara, USA). The ferroelectric polarization hysteresis (*P*-*E*) loops and strain–electric field (*S*–*E*) curves were measured using a ferroelectric testing system (TF Analyzer 3000E, aixACCT, Aachen, Germany). The electromechanical coupling factor k_p and the mechanical quality factor Q_m were calculated based on the resonance anti-resonance method by utilizing the same instrument of Agilent 4294A, and the calculation formulas are shown in (1) and (2).

$$\frac{1}{k_p{}^2} = 0.398\frac{f_r}{f_a - f_r} + 0.579, \tag{1}$$

$$Q_m = \frac{f_a{}^2}{2\pi f_r RC\left(f_a{}^2 - f_r{}^2\right)}, \tag{2}$$

where f_r is the resonance frequency and f_a is the anti-resonance frequency, respectively. R is the impedance at f_r and C is the electric capacitance at 1 kHz.

3. Results and Discussion

Figures 1(a) and 1(b) show the X-ray diffraction (XRD) spectra of BS–*y*PT–*x*BMS ceramics at room temperature. There is no evidence of secondary phase or any other impurity, indicating that BMS end member successfully enters into the BS–PT solid solution and a stable single-phase perovskite structure is formed. From the XRD patterns with x value of 0.005 in Figs. 1(a) and 1(a′), it can be seen that the asymmetry of (111) is absent and the (200) peak is split into (002) and (200) gradually as the PT content increases from 0.630 to 0.645, indicating a transition from coexistence of two phases to tetragonal phase. To further investigate the detailed phase structures of BS–*y*PT–0.005BMS ceramics, the Rietveld refinement was performed using the model of *R*3*m* and

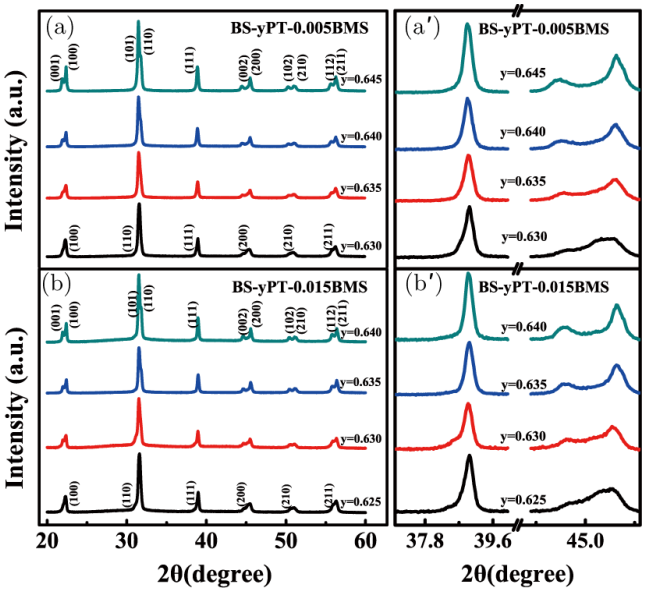

Fig. 1. XRD patterns of BS–*y*PT–*x*BMS: (a) x = 0.005, y = 0.630–0.645; (b) x = 0.015, y = 0.625–0.640; (a′) and (b′) the corresponding magnified patterns of (a) and (b) in the vicinity of 2θ = 37°–46°.

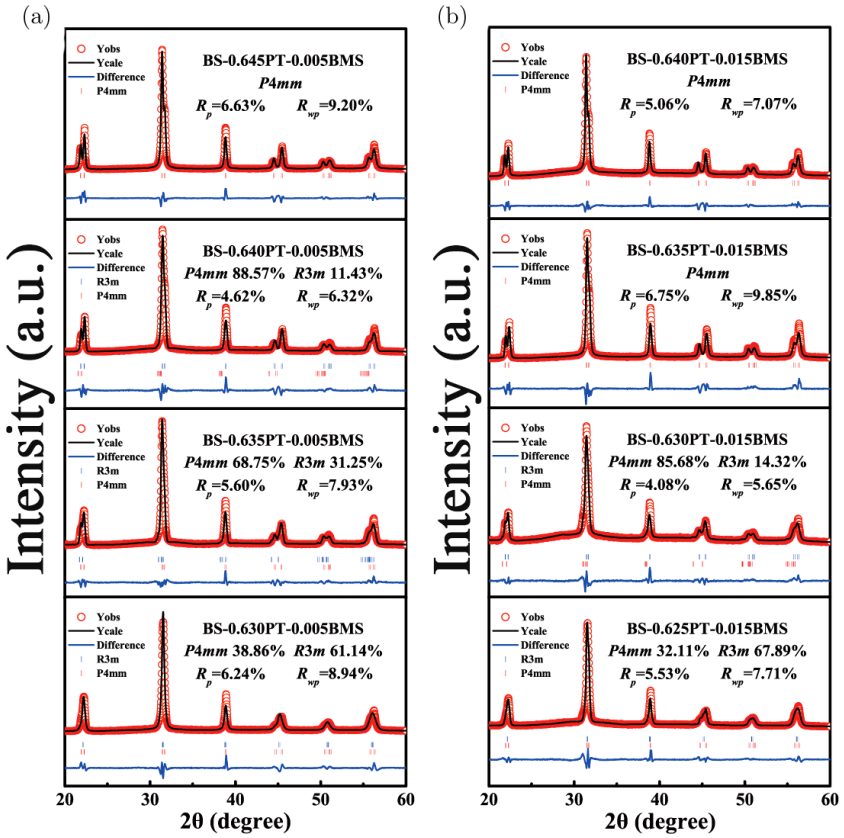

Fig. 2. Rietveld refinement results of (a) BS–0.640PT–0.005BMS and (b) BS–0.630PT–0.015BMS ceramics.

*P*4*mm* phases as shown in Fig. 2(a). The Rietveld refinement results show that the samples with y = 0.630–0.640 are corresponding to the coexistence of *R*3*m* and *P*4*mm* phases, that is, the MPB region locates at y = 0.630–0.640. Combined with Table 1, it can be found that the MPB composition at y = 0.640 obtains the optimal piezoelectric properties of d_{33} = 221 pC/N and k_p = 0.335. The similar changing phenomenon also occurs in BS–*y*PT–0.015BMS ceramics as shown in Figs. 1(b) and 1(b′) and Fig. 2(b), and the MPB region exists at y = 0.630 vicinity. Compared with the MPB composition for 0.36BS–0.64PT,[15] the addition of 0.5 mol.% BMS almost has no impact on PT content for MPB. However, with the increase of BMS to 1.5 mol.%, the composition of MPB moves towards the area with low PT content of 0.630. For the samples with a certain content of BMS, the increase of PT content can result in the strengthening of tetragonality, and this in turn will affect the electrical performances.

Figure 3 shows the typical fracture morphologies of sintered BS–*y*PT–*x*BMS ceramics. All ceramic samples are relatively compact with no obvious pores. The grain diameter of each sample is calculated and the variation of average grain size with PT content of 0.5 mol.% BMS and 1.5 mol.%

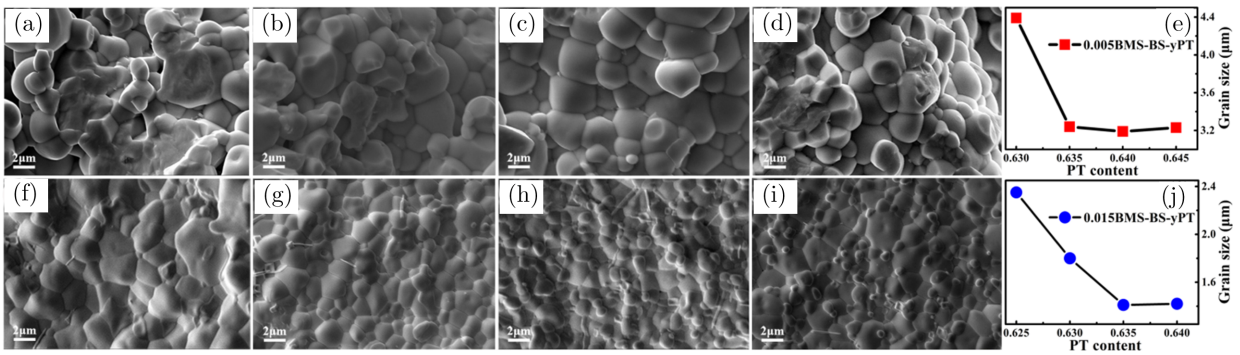

Fig. 3. The fracture surfaces SEM images of (a–d) BS–*y*PT–0.005BMS (y = 0.630–0.645) and (e–h) BS–*y*PT–0.015BMS (y = 0.625–0.640); the average grain size of (e) BS–*y*PT–0.005BMS and (j) BS–*y*PT–0.015BMS.

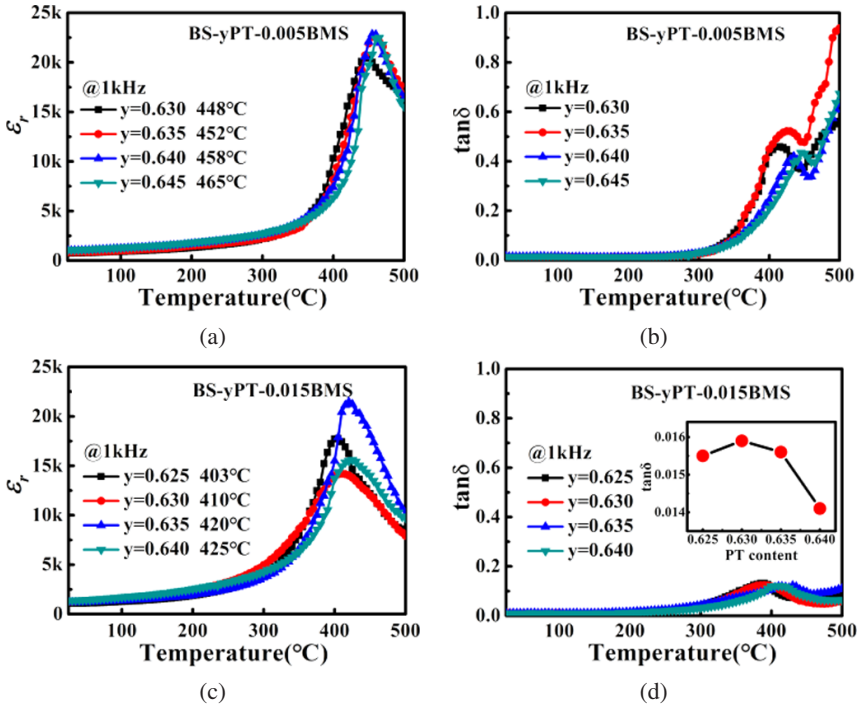

Fig. 4. Temperature-dependent ε_r and tanδ: (a) and (b) BS–yPT–0.005BMS ceramics, and (c, d) BS–yPT–0.015BMS ceramics; The inset in (d) is the tanδ of BS–yPT–0.015BMS ceramics with different PT contents at 200°C.

BMS-doped ceramics are shown in Figs. 3(e) and 3(j). It can be easily seen that the average grain size possesses little change for the samples with the same BMS content no matter how the PT content changes. However, with the increase of BMS doping amount from 0.005 to 0.015, the average grain size has a decreasing tendency from 3.19–4.39 μm to 1.41–2.35 μm. The BMS can prevent grain boundary movement and inhibit grain growth during sintering, and accordingly lead to grain refinement. Similar phenomenon can also be observed in the previous Sb-doped BS–PT-based system.[27] Therefore, the morphology of BS–yPT–xBMS ceramic is sensitive to the BMS content but not to the PT content. In addition, the crystal fracture follows the lowest energy interface. The intergranular fracture mode exhibits when the mechanical strength of grain is stronger than the grain boundary, whereas the transgranular fracture mode occurs.[28] For all of BS–yPT–xBMS samples, the relatively low grain growth speed and a small grain size make the mechanical strength of the grain stronger than the grain boundary, resulting in the dominant intergranular fracture mode.

Temperature dependence of the dielectric permittivity (ε_r) and dielectric loss (tanδ) at 1 kHz frequency for BS–yPT–0.005BMS and BS–yPT–0.015BMS samples has been shown in Fig. 4. The temperature corresponding to the maximum value of ε_r is considered as Curie temperature T_C. The T_C of each sample is above 400°C, which meets the most important performance requirements of high-temperature devices working at ~200°C. Due to the high phase transition temperature of 490°C for $PbTiO_3$ ceramics, the T_C increases with the PT content increasing for BS–yPT–0.005BMS or 0.015BMS ceramics, as shown in Figs. 4(a) and 4(c). Also, the increase of BMS introduction leads to the decrease of T_C to some extent. Taking the MPB compositions for example, T_C value (458°C) of BS–0.640PT–0.005BMS is much higher than that of BS–0.630PT–0.015BMS (410°C).

From the tanδ as a result of temperature, it can be seen that each sample has low tanδ values below 1.5% at room temperature and even maintain ~1.60% at a high temperature of 200°C. Compared with the pure 0.36BS–0.64PT ceramic with high tanδ (> 3%@25°C),[15] the addition of BMS can reduce tanδ effectively. According to the defect chemistry theory, B-site ions such as Ti^{4+} and Sc^{3+} in BS–PT phase replaced by low valence $Mn^{2+,3+}$ due to the introduction of BMS, can produce oxygen vacancies, thus inhibiting the movement of domain walls and reducing the dielectric loss.[29] When the addition amount of BMS changes from 0.5 mol.% to 1.5 mol.%, the tanδ further decreases in the overall testing temperature range. More oxygen vacancies were generated in BS–yPT–0.015BMS ceramics. And hence the dielectric loss is further reduced. Generally speaking, piezoelectric ceramics have prominent piezoelectric properties near MPB, but tanδ values are high simultaneously.[15,30] In this work, for BS–0.630PT–0.015BMS, the values of tanδ are only 1.2%@25°C and 1.59%@200°C as shown in the inset of Fig. 4(d), which are very beneficial to inhibit the thermal failure of piezoelectric devices.

Figures 5(a) and 5(d) show the polarization hysteresis (P-E) loops of the BS–yPT–xBMS ceramics measured at

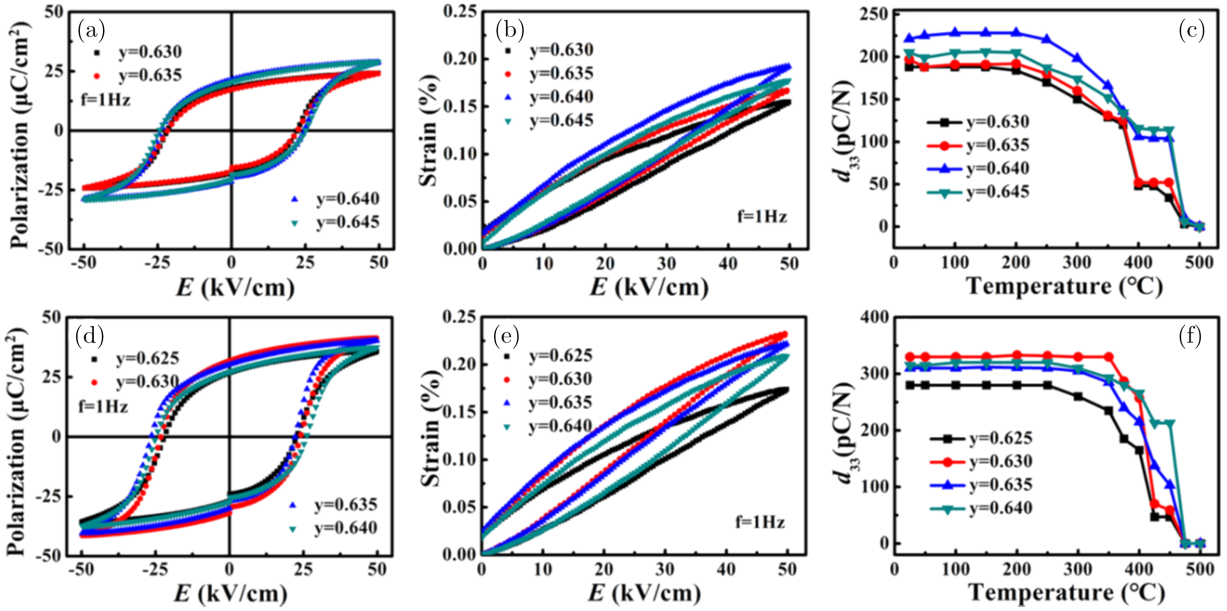

Fig. 5. *P–E* hysteresis loops, *S–E* curves and temperature-dependence *ex situ* d_{33} of (a–c) BS–*y*PT–0.005BMS and (d–f) BS–*y*PT–0.015BMS.

1 Hz under the same electric field of 50 kV/cm at room temperature. All *P-E* loops are symmetrical without obvious conduction phenomenon, showing typical ferroelectric features. Clearly, with the same content of BMS, the remnant polarization P_r increases firstly, and reaches a maximum value at MPB composition, and then decreases with the increasing PT content. Meanwhile, the ferroelectric properties are sensitive to the BMS doping amount. With the increase of BMS, BS–*y*PT–0.015BMS ceramics show enhanced ferroelectric performance characterized by high polarization. The values of P_r and *Ec* of BS–*y*PT–0.005BMS and BS–*y*PT–0.015BMS series range from 17.4 to 20.8 μC/cm^2 and 16.4–21.8 kV/cm, 26.8–31.9 μC/cm^2 and 22.1–26.2 kV/cm, respectively.

The unipolar strain–electric field (*S–E*) curves of the poled BS–*y*PT–*x*BMS specimens are measured under the high electric field of 50 kV/cm and shown in Figs. 5(b) and 5(e). The electric field-induced unipolar strain of BS–*y*PT–0.005BMS ceramics increases with PT content increasing, and reaches a maximum value of 0.19% at $y = 0.640$, then decreases as the PT content further increases. However, for BS–*y*PT–0.015BMS ceramics, a much higher value of 0.23% can be obtained at $y = 0.630$. The maximum strain value at MPB can be interpreted as the enhanced polarizability and domain wall mobility where large numbers of thermodynamically stable polarization directions exist.[31,32]

Thermal depoling temperature of piezoelectric ceramics determines the service temperature of their applications. Therefore, in order to prove the stability of piezoelectric properties of BS–*y*PT–*x*BMS at high temperature, the piezoelectric constant d_{33} of all ceramic samples was measured at room temperature after annealed treatment at various temperatures for 30 min. Figures 5(c) and 5(f) display the influence of thermal depolarization from room temperature to 500°C on the piezoelectric coefficient d_{33} of BS–*y*PT–0.005BMS and BS–*y*PT–0.015BMS ceramics. It is clearly seen that the d_{33} values of 0.5 mol.% BMS-doped ceramics are basically unchanged below 200°C, and then begin to reduce rapidly to zero as the temperature increases to the vicinity of T_C. While for 0.015 mol.% BMS-doped ceramics, the change tendency of d_{33} values with temperature increasing is similar to that of BS–*y*PT–0.005BMS. It can be noted that a large *ex situ* d_{33} of ~330 pC/N for BS–0.63PT–0.015BMS can remain almost unchanged below 350°C, which guarantees the stability of piezoelectric performance at high temperatures.

As the BS–0.630PT–0.015BMS ceramic sample shows enhanced ferroelectric polarization, *ex situ* d_{33} and piezoelectric strain, the *in situ P-E* and *S-E* measurements are carried out for further investigation. Figure 6(a) displays the polarization–electric field (*P–E*) hysteresis loops of the BS–0.630PT–0.015BMS ceramics from 25°C to 200°C at 1 Hz under the applied electric field of 30 kV/cm. For avoiding the thermal breakdown, the test voltage is set to 60% of that at room temperature. The changes for two main performance parameters of P_r and E_c at various temperatures are extracted and shown in Fig. 6(b). With the increase of temperatures, the P_r increases slightly from 25.5 to 28.6 μC/cm^2, while E_c decreases from 19.3 to 10.9 kV/cm when the measuring temperature changes in the range of 25–200°C. Figure 6(c) exhibits the unipolar strain curves of BS–0.630PT–0.015BMS ceramic at various temperatures under a certain electric field of 30 kV/cm and frequency of 1 Hz. With the temperature increasing from 25°C to 200°C, the electric field-induced unipolar strain gradually increases, and reaches to 0.202% at 200°C, which is about 1.6 times more than the value of 0.124% at room temperature. The inverse piezoelectric

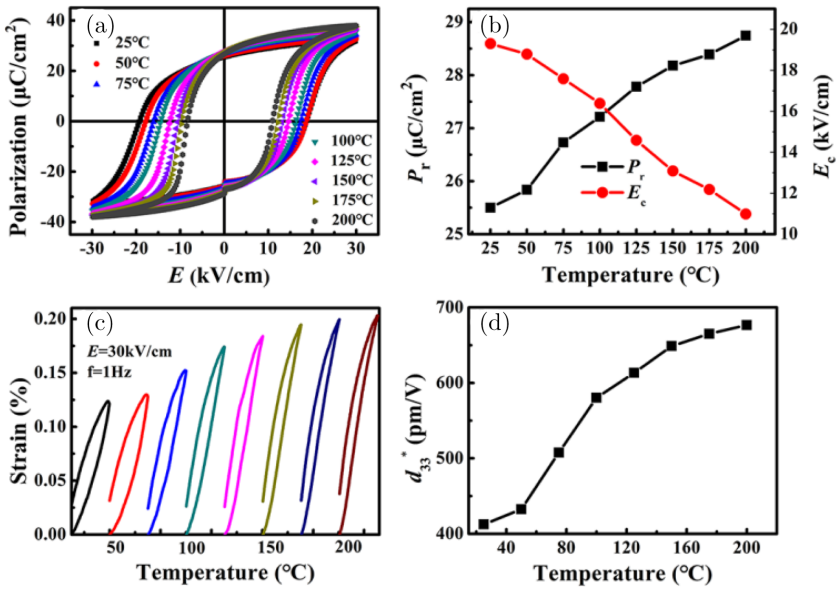

Fig. 6. The *P–E* and *S–E* curves for BS–0.63PT–0.015BMS ceramics measured from 25°C to 200°C at 1Hz under 30 kV/cm: (a) *P–E* loops, (b) P_r and E_c, (c) unipolar strain curves, and (d) d_{33}^* values.

coefficient d_{33}^* is calculated and plotted in Fig. 6(d). The d_{33}^* value increases monotonously from 412 pm/V to 676 pm/V when the temperature increases from 25°C to 200°C. The above phenomenon can be explained that more ferroelectric domains are activated and domain wall motion is enhanced at higher temperatures.[33,34]

Table 1 summarizes the piezoelectric and dielectric properties of BS–*y*PT–*x*BMS ceramics in detail. It can be found that both 0.5 mol.% BMS and 1.5 mol.% BMS-doped ceramics achieve the optimal properties at MPB compositions. For ceramics with BMS content of 0.5%, the T_C is kept around 450°C, but d_{33} is drastically reduced, even less than half of pure 0.36BS–0.64PT ceramic (d_{33} = 460 pC/N).[15] Fortunately, with the addition of BMS increasing to 1.5 mol.%, T_C only drops a little but still remains above 400°C, and d_{33} is above 300 pC/N. For BS–0.630PT–0.015BMS, the outstanding comprehensive performances can be achieved with d_{33} = 330 pC/N, k_p = 0.498, tanδ = 1.59% (@200°C), Q_m = 84, ε_r =1384, and T_C = 410°C.

In order to evaluate the piezoelectric performances for the best BS–0.630PT–0.015BMS sample, a statistical summary of d_{33}, T_C, and tanδ comparison between this work and some previously reported BS–PT based piezoelectric ceramics is made as illustrated in Fig. 7. As shown, the tanδ of BS–0.630PT–0.015BMS is much lower than those of BNZ–BSPT(tanδ = 4.3%), PSN–BSPT (tanδ = 4.1%), PZN–BSPT(tanδ = 2.4%), and BMTFS–PT (tanδ = 3.6%). By comparison, the PMS–BSPT have relatively reduced tanδ, but at the expense of T_C (365°C). Also, under the condition of T_C greater than 400°C, two key parameters of d_{33} and tanδ for BS–0.630PT–0.015BMS (d_{33} = 330 pC/N, tanδ = 1.2%) are better than those of PMN–BSPT (d_{33} = 300 pC/N, tanδ = 1.5%) and BSPT–4%Fe (d_{33} = 301 pC/N, tanδ = 2.2%). Thus, among the high-temperature piezoelectric ceramics,

Table 1. Electrical properties of BS–*y*PT–*x*BMS ceramics.

BS–*y*PT–*x*BMS	d_{33} (pC/N) 25°C	d_{33}^* (pm/V)	k_p	tanδ (%) 25°C	tanδ (%) 200°C	Q_m	ε_r	T_C (°C)	ρ (g/cm^3)
x = 0.005, y = 0.630	188	516	0.296	1.20	1.27	85	755	448	6.700
x = 0.005, y = 0.635	197	557	0.305	1.26	1.28	82	853	452	6.320
x = 0.005, y = 0.640	221	641	0.335	1.50	1.35	65	1028	458	7.369
x = 0.005, y = 0.645	205	591	0.329	1.32	1.30	76	1013	465	6.985
x = 0.015, y = 0.625	280	580	0.441	0.90	1.55	117	1000	403	5.854
x = 0.015, y = 0.630	330	775	0.498	1.20	1.59	84	1384	410	7.271
x = 0.015, y = 0.635	310	739	0.468	1.10	1.56	109	1267	420	6.273
x = 0.015, y = 0.640	315	695	0.447	1.00	1.41	101	1126	425	6.909

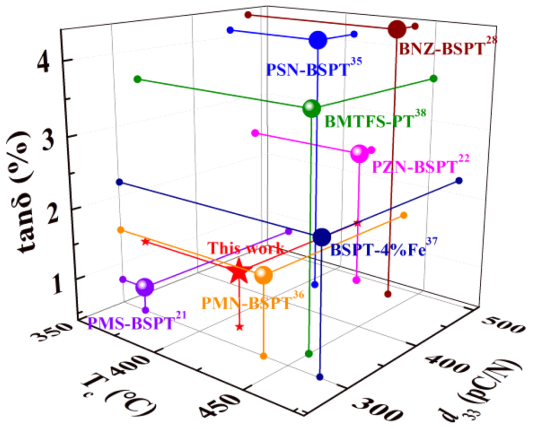

Fig. 7. Comparisons of piezoelectric properties for this work with other BS–PT-based piezoelectric ceramic.

BS–0.630PT–0.015BMS ceramic shows great advantages in high-temperature applications because of its good balance among the values of d_{33}, T_C and tanδ.

4. Conclusion

In summary, a novel BS–yPT–xBMS high-temperature piezoelectric ceramic system was designed and prepared by the traditional solid-state reaction method. Compared with other compositions, BS–0.630PT–0.015BMS at MPB possesses the optimal electrical properties with d_{33} of 330 pC/N, T_C of 410°C, ε_r of 1384, Q_m of 84, and tanδ of 1.20%. The introduction of BMS reduces the dielectric loss, and increases the mechanical quality factors, which is a great improvement in comparison with pure BS–PT ceramics. Moreover, BS–0.630PT–0.015BMS ceramics maintain both a high Curie temperature ($T_C > 400$°C) and excellent piezoelectric properties ($d_{33} > 300$ pC/N). These results demonstrate that BS–0.630PT–0.015BMS has great potential as the functional material of piezoelectric devices in high-temperature applications.

Acknowledgments

This work was supported by the National Natural Science Foundation of China (Grant Nos. 51972144, U1806221 and U2006218), the Taishan Scholars Program, the Case-by-Case Project for Top Outstanding Talents of Jinan, the Shandong Provincial Natural Science Foundation (Grant No. ZR2020KA003), the Primary Research & Development Plan of Shandong Province (Grant No. 2019JZZY010313), the Project of "20 Items of University" of Jinan (Grant Nos. T202009 and T201907), and the Introduction Program of Senior Foreign Experts (G2021024003L).

References

[1]S. J. Zhang and F. P. Yu, Piezoelectric Materials for High Temperature Sensors, *J. Am. Ceram. Soc*. **94**, 3153 (2011).
[2]D. Darnjanovic, Materials for high temperature piezoelectric transducers, *Solid State Mater. Sci*. **3**(5), 469 (1998).
[3]J. G. Chen, J. R. Cheng and S. X. Dong, Review on high temperature piezoelectric ceramics and actuators based on $BiScO_3$–$PbTiO_3$ solid solutions, *J. Adv. Dielectr*. **4**(1), 1430002 (2014).
[4]S. J. Zhang, X. M. Jiang, M. Lapsley, P. Moses and T. R. Shrout, Piezoelectric accelerometers for ultrahigh temperature application, *Appl. Phys. Lett*. **96**(1), 013506 (2010).
[5]C. Feng, Y. Y. Feng, M. J. Fan, C. H. Geng, X. J. Lin, C. H. Yang and S. F. Huang, $BiScO_3$–$BiFeO_3$–$PbTiO_3$–$BaTiO_3$ high-temperature piezoelectric ceramic and its application on high-temperature acoustic emission sensor, *J. Cent. South Univ*. **28**, 3747 (2021).
[6]S. X. Dong, Review on piezoelectric, ultrasonic, and magnetoelectric actuators, *J. Adv. Dielectr*. **2**, 1230001 (2012).
[7]A. Benčan, B. Malič, S. Drnovšek, J. Tellier, T. Rojac, J. Pavlič, M. Kosec, K. G. Webber, J. Rödel and D. Damjanovič, Structure and the electrical properties of $Pb(Zr,Ti)O_3$–Zirconia composites, *J. Am. Ceram. Soc*. **95**(2), 651 (2012).
[8]Z. Q. Hu, J. G. Chen, M. Y Li, X. T Li, G. X. Liu and S. X. Dong, Morphotropic phase boundary and high temperature dielectric, piezoelectric, and ferroelectric properties of $(1–x)Bi(Sc_{3/4}In_{1/4})O_3$–$xPbTiO_3$ ceramics, *J. Appl. Phys*. **110**(6), 064102 (2011).
[9]R. C. Turner, P. A. Fuierer, R. E. Newnham and T. R. Shrot, Materials for high temperature acoustic and vibration sensors: A Review, *Appl. Acoust*. **41**(4), 299 (1994).
[10]Z. Gubinyi, C. Batur, A. Sayir and F. Dynys, Electrical properties of PZT piezoelectric ceramic at high temperatures, *J. Electroceram*. **20**(2), 95 (2008).
[11]D. V. Kuzenko, Temperature-activation mechanism of the temperature dependence of the dielectric constant of ferroelectric ceramics PZT, *J. Adv. Dielectr*. **12**, 2250010 (2022).
[12]Q. Wang, C. M. Wang, J. F. Wang and S. J. Zhang, High performance Aurivillius-type bismuth titanate niobate (Bi_3TiNbO_9) piezoelectric ceramics for high temperature applications, *Ceram. Int*. **42**(6), 6993 (2016).
[13]C. M. Wang, L. Zhao, Y. Liu, R. L. Withers, S. J. Zhang and Q. Wang, The temperature-dependent piezoelectric and electromechanical properties of cobalt-modified sodium bismuth titanate, *Ceram. Int*. **42**(3), 4268 (2015).
[14]R. E. Eitel, C. A. Randall, T. R. Shrout, P. W. Rehrig, W. Hackenberger and S. E. Park, New high temperature morphotropic phase boundary piezoelectrics based on $Bi(Me)O_3$–$PbTiO_3$ ceramics, *Jpn. J. Appl. Phys*. **40**(10), 5999 (2001).
[15]R. E. Eiltel, C. A. Randall, T. R. Shrout, S. E. Park, Preparation and characterization of high temperature perovskite ferroelectrics in the solid-solution $(1–x)BiScO_3$–$xPbTiO_3$, *Jpn. J. Appl. Phys*. **41**(4), 2099 (2002).
[16]E. D. Politova, G. M. Kaleva, A. V. Mosunov, A. H. Segalla, A. E. Dosovitskiy and A. L. Mikhlin, Processing, phase transitions, and dielectric properties of BSPT ceramics, *J. Adv. Dielectr*. **3**(3), 1350024 (2013).
[17]R. E. Eitel, T. R. Shrout and C. A. Randall, Tailoring properties and performance of $(1–x)BiScO_3$–$xPbTiO_3$ based piezoceramics by Lanthanum Substitution, *Jpn. J. Appl. Phys*. **43**(12), 8146 (2004).
[18]A. Sehirlioglu, A. Sayir and F. Dynys, Doping of $BiScO_3$–$PbTiO_3$ Ceramics for Enhanced Properties, *J. Am. Ceram. Soc*. **93**(6), 1718 (2010).
[19]S. J. Zhang, R. E. Eitel, C. A. Randall and T. R. Shrout, Manganese-modified $BiScO_3$–$PbTiO_3$ piezoelectric ceramic for high-temperature shear mode sensor, *Appl. Phys. Lett*. **86**(26), 262904 (2005).
[20]I. Sterianou, I. M. Reaney, D. C. Sinclair, D. I. Woodward, D. A. Hall, A. J. Bell and T. P. Comyn. High-temperature (1–x)-

$BiSc_{1/2}Fe_{1/2}O_3$–$x$$PbTiO_3$ piezoelectric ceramics, *Appl. Phys. Lett*. **87**(24), 242901 (2005).

[21]B. L. Deng, Q. Wei, C. He, Z. J. Wang, X. M. Yang and X. F Long, Effect of $Pb(Mn_{1/3}Sb_{2/3})O_3$ addition on the electrical properties of $BiScO_3$–$PbTiO_3$ piezoelectric ceramics, *J. Alloys Compd*. **28**(790), 397 (2019).

[22]Z. H. Yao, H. X. Liu, H. Hao and M. H. Cao, Structure, electrical properties, and depoling mechanism of $BiScO_3$–$PbTiO_3$–$Pb(Zn_{1/3}Nb_{2/3})O_3$ high-temperature piezoelectric ceramics, *J. Appl. Phys*. **109**(1), 014105 (2011).

[23]C. J. Stringer, T. R. Shrout and C. A. Randall, High-temperature perovskite relaxor ferroelectrics: A comparative study, *J. Appl. Phys.* **101**(5), 054107 (2007).

[24]W. J. Qian, Y. Yang, Y. P. Wang, B. Wang and L. L. Liu. Structure and electrical properties of $0.07Pb(Mn_{1/3}Sb_{2/3})O_3$–$(0.93–x)$ $BiScO_3$–$x$$PbTiO_3$ piezoelectric ceramics, Symposium on Piezoelectricity, Acoustic Waves and Device Applications, April 2011.

[25]M. R. Suchomel and P. K. Davies, Enhanced tetragonality in xPb-TiO_3–$(1–x)Bi(Zn_{1/2}Ti_{1/2})O_3$ and related solid solution systems, *Appl. Phys. Lett.* **86**, 262905 (2005).

[26]A. Sehirlioglu, A. Sayir and F. Dynys, Doping of $BiScO_3$–$PbTiO_3$ Ceramics for Enhanced Properties, *J. Am. Ceram. Soc.* **93**(6), 1718 (2010).

[27]L Xue, Q Wei, Z. J. Wang, X. M. Yang, X. F. Long and C. He, Electrical properties of Sb_2O_3-modified $BiScO_3$–$PbTiO_3$-based piezoelectric ceramics, *RSC Adv*. **10**(23), 13460 (2020).

[28]T. L. Zhao, C. L. Fei, K. W. Pu, X. Y. Dai, J. J. Song, C. M. Wang and S. X. Dong, Structure evolution and enhanced electrical performance for $BiScO_3$–$Bi(Ni_{1/2}Zr_{1/2})O_3$–$PbTiO_3$ solid solutions near the morphotropic phase boundary, *J. Alloys Compd*. **873**, 159844 (2021).

[29]Y Yu, J. K. Yang, J. G. Wu, X. Y. Gao, L. Bian, X. T. Li, X. D. Xin, Z. H. Yu, W. P. Chen and S. X. Dong, Ultralow dielectric loss of $BiScO_3$–$PbTiO_3$ ceramics by $Bi(Mn_{1/2}Zr_{1/2})O_3$ modification*, J. Eur. Ceram. Soc*. **40**(8), 3003 (2020).

[30]T. L. Zhao, C. L. Fei, X. Y. Dai, J. J. Song and S. X. Dong, Structure and enhanced piezoelectric performance of $BiScO_3$–$PbTiO_3$–$Pb(Ni_{1/3}Nb_{2/3})O_3$ ternary high temperature piezoelectric ceramics, *J. Alloys Compd*. **806**, 11 (2019).

[31]J. G. Chen, T. L. Zhao, J. R. Cheng and S. X. Dong, Enhanced piezoelectric performance of $(0.98–x)Bi(Sc_{3/4}In_{1/4})O_3$–$x$Pb-$TiO_3$–$0.02Pb(Zn_{1/3}Nb_{2/3})O_3$ ternary high temperature piezoelectric ceramics, *J. Appl. Phys.* **113**(14), 144102 (2013).

[32]T. L. Zhao, J. G. Chen, C. M. Wang, Y. Yu and S. X. Dong, Ferroelectric, piezoelectric, and dielectric properties of $BiScO_3$–$PbTiO_3$–$Pb(Cd_{1/3}Nb_{2/3})O_3$ ternary high temperature piezoelectric ceramics, *J. Appl. Phys*. **114**(2), 027014 (2013).

[33]N. N. Wathore, C. M. Lonkar and D. K. Kharat, Effect of temperature on polarization reversal of strontium-doped lead zirconate titanate (PSZT) ceramics, *Bull. Mater. Sci*. **34**(1), 129 (2011).

[34]R. A. Malik, A. Hussain, A. Maqbool, A. Zaman, C. W. Ahn, J. U. Rahman, T. K. Song, W. J. Kim and M. H. Kim, Temperature-Insensitive High Strain in Lead-Free $Bi_{0.5}(Na_{0.84}K_{0.16})_{0.5}TiO_3$–$0.04SrTiO_3$ Ceramics for Actuator Applications, *J. Am. Ceram. Soc.* **98**(12), 3842 (2015).

[35]Z. H. Yao, H. X. Liu, Y. Liu, Z. Li, X. B. Cheng, M. H. Cao and H. Hao, Morphotropic phase boundary in $Pb(Sc_{1/2}Nb_{1/2})O_3$–$BiScO_3$–$PbTiO_3$ high temperature piezoelectrics, *Mater. Lett*. **62**(29), 4449 (2008).

[36]J. G. Chen, Y. J. Dong and J. R. Cheng, Reduced dielectric loss and strain hysteresis in $(0.97–x)BiScO_3$–$x$$PbTiO_3$–$0.03Pb(Mn_{1/3}Nb_{2/3})O_3$ piezoelectric ceramics, *Ceram. Int*. **41**(8), 9828 (2015).

[37]J. G. Wu, Y. Yu, X. T. Li, X. Y. Gao and S. X. Dong, Investigation on Resonant Vibration Performances of Fe-Doped $BiScO_3$–$PbTiO_3$ Ceramics in High-Temperature Environment, *J. Am. Ceram. Soc*. **98**(10), 3145 (2015).

[38]T. Sebastian, I. Sterianou, D. C. Sinclair, A. J. Bell, D. A. Hall and I. M. Reaney, High temperature piezoelectric ceramics in the $Bi(Mg_{1/2}Ti_{1/2})O_3$–$BiFeO_3$–$BiScO_3$–$PbTiO_3$ system, *J. Electroceram.* **25**(2–4), 130 (2010).